A New Adaptive Double Envelope Feedback (ADEF) Linearizer for Solid State Power Amplifiers

Jean-Serge Cardinal and Fadhel M. Ghannouchi, *Senior Member, IEEE*

Abstract—**A new adaptive double envelope feedback (ADEF) linearizer using a voltage-controlled phase-shifter for predistortion purpose and a dynamic gate bias for gain stabilization purpose has been developed and implemented on a two-watt MESFET amplifier. A two-tone test around 1.6 GHz shows average in-band intermodulation product below −40 dBc up to saturation with a power-added efficiency of 40% at the 1-dB compression point. Validation of the adaptive features of the ADEF technique is carried out with respect to carrier frequency, temperature, two-tone amplitude offset and spacing. In addition, a new formula, which directly relates the third order intermodulation level to the AM/AM and AM/PM distortion coefficients of solid state nonlinear amplifiers is proposed and its accuracy is assessed using both simulation and experimental results.**

I. Introduction

DIGITAL mobile radio services using $\pi/4$-DQPSK modulated signals with an output power of approximately one watt are already in use in Europe [1], Japan [2] and North America [3]. This application requires power amplifiers that are highly linear [4], power efficient and insensitive to outdoor temperature variations and battery level drifts. Intensive research is being carried out to develop new linearization techniques that optimize the trade-off between the In-Band Intermodulation Products (IBIP) versus Power-Added Efficiency (PAE). The following is a brief list of the most efficient techniques:

1) Linear saturated amplifier with bi-directional control (LSA-BC) [5]: a dynamic bias on the drain combined with envelope feedback on the gain.
2) LInear amplifiers using nonlinear components (LINC) [6]: the QPSK modulated signal is converted into two constant-amplitude phase modulated signals that drive two saturated amplifiers. The output of the amplifiers are then combined to reproduce the QPSK signal.
3) Cartesian feedback [7]: the output signal is demodulated and compared to the input baseband signal. The resulting predistorted signal is remodulated and amplified by the saturated amplifiers.
4) Adaptive predistortion [8]: the baseband signal is predistorted by a digital signal processor (DSP), modulated and amplified by a saturated amplifier. The output is demodulated and processed by a DSP in order to correct for the amplifier nonlinearities.
5) Feedforward [9]: a sample of the amplifier output IBIP components are amplified, phase inverted and nullified at the output coupler.

All of these methods, and several of their variations, have shown very good IBIP suppression results but at the price of highly complex systems. Their efficiency and physical size are degraded by high-speed dc-to-dc converters, DSP circuits or auxiliary RF amplifiers which do not contribute to the output power. Furthermore, variations in environmental conditions degrade the IBIP performance of nonadaptive linearizers such as LINC or Feedforward. Finally, memory effects that degrade the AM/AM and AM/PM distortion levels can also be a serious problem for linearizers based on predistortion such as LINC or Feedforward [10].

In the quest for a new approach for linearizers where circuit simplicity, PAE, IBIP, and adaptability are the main concerns, a new adaptive double envelope feedback (ADEF) linearized amplifier has been developed. This approach combines dynamic biasing, phase predistortion, and envelope feedback techniques [11]–[13]. A prototype has been designed, manufactured and tested. Promising results have been obtained.

II. Design Principles

It is well known that the intermodulation products at the output of a power amplifier driven by a multitone signal results from the AM/AM and AM/PM distortion of this power amplifier. The implementation of the ADEF technique require the knowledge of the maximum levels of AM/AM and AM/PM distortions in order to design the feedback loops that maintain C/I_3 below the target specification.

A. Third-Order Nonlinearities versus AM/AM and AM/PM Conversion Coefficients

The level of the third order intermodulation products relative to the carrier's in two-tone test, for a given average input power level, P'_{in} in watts, can be calculated by means of the following [14]

$$\frac{C}{I_3} \approx -10 \log \left[\left(\frac{P'_{\text{in}} G'_1}{2G'_0} \right)^2 + \left(\frac{P'_{\text{in}} A'_1}{2} \right)^2 \right] \qquad (1)$$

where G'_1, A'_1 are the AM/AM, AM/PM conversion coefficients in (V/V W) and (radian/watt), respectively, and G'_0 is the small signal gain in (V/V) of a hypothetical black box amplifier model (BBAM's) as shown in Fig. 1(a).

Manuscript received August 1, 1994; revised December 19, 1994. This work was supported by the Natural Science and Engineering Council of Canada, Grant 0118056.

J.-S. Cardinal was with the Electrical and Computer Engineering Department, École Polytechnique de Montréal, University of Montréal. He is now with SR Teleocm, Montréal, Québec, Canada.

F. M. Ghannouchi is with the Electrical and Computer Engineering Department, École Polytechnique de Montréal, University of Montréal, Montréal, Canada.

IEEE Log Number 9412033.

TABLE I
COMPARISON OF THE VALUES OF C/I_3 OBTAINED USING (3) AND (4) AND MDS RESULTS

G_1 (dB/dB)	A_1 (deg/dB)	C/I3 by (3) (dBc)	C/I3 by (4) (dBc)	C/I3 by sim. (dBc)
0	0.06	-52.49	-50.64	-50.67
0	0.2	-42.38	-40.54	-40.56
0	1	-28.4	-26.55	-26.58
0	2	-22.38	-20.54	-20.56
0.03	0	-42.14	-41.8	-40.36
0.03	0.06	-41.76	-41.3	-39.98
0.06	0	-36.12	-35.78	-34.4
0.13	0	-30.1	-29.76	-28.5
0.13	0.25	-29.72	-29.23	-28.11
0.25	0	-24.08	-23.74	-22.71
0.5	0	-18.06	-17.72	-17.16
0.5	1	-17.68	-17.19	-16.77
1	0	-12.04	-11.7	-12.04
1	2	-11.66	-11.17	-11.67
2	4	-5.64	-5.15	-7.36

In particular, for smooth gain and phase variations around a given input power level, the new AM/AM and AM/PM coefficients G_1 and A_1 respectively can be derived where G_1 is in dB/dB and A_1 in deg/dB as shown in Fig. 1(b). Based on this transformation (1) can be rearranged in the following way

$$\frac{C}{I_3} = -10\log\left[\left(\frac{0.25G_1}{1-\frac{G_1}{2}}\right)^2 + (0.038A_1)^2\right]. \quad (2)$$

Furthermore, for small gain variations around a given output power level ($G1 \ll 1$ dB/dB), (2) can be approximated by

$$\frac{C}{I_3} \approx -10\log\lfloor(0.25G_1)^2 + (0.038A_1)^2\rfloor. \quad (3)$$

A systematic investigation of a black box amplifier model (BBAM) based on computer simulations and an experimental verification has been conducted with the purpose of refining (3) in order to cover a wider dynamic range. The BBAM is depicted in Fig. 1(b) and consists of prescribed AM/AM, G_1, and AM/PM, A_1, distortion coefficients. The simulation procedure consists of applying a two-tone harmonic balance analysis to the BBAM and extracting the C/I_3 ratio from the results. This investigation has led us to the following improved formula:

$$\frac{C}{I_3} = -10\log\lfloor(0.26G_1)^2 + (0.047A_1)^2\rfloor \quad (4)$$

which yields more accurate results over a wider dynamic range, from -50 to -10 dBc backoff power level relative to 1 dB compression point, $P_{1\text{dB}}$, as illustrated by Table I. These results are confirmed further by the experimental validation of (4) which is given in Section V-B.

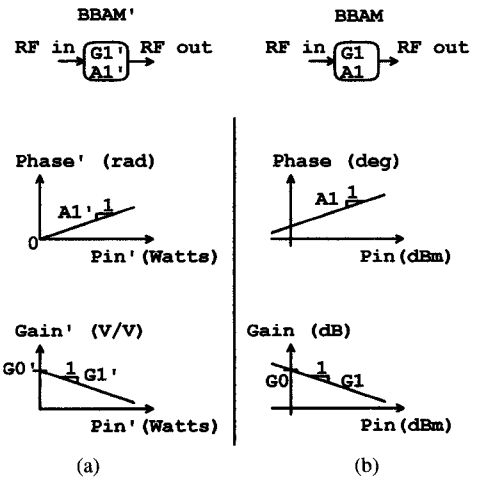

Fig. 1. (a) A black box model of a nonlinear amplifier (BBAM) with its AM/AM and AM/PM distortion coefficients in (V/V W) and (Rad/V). (b) A black box model of a nonlinear amplifier (BBAM) with its AM/AM and AM/PM distortion coefficients in (dB/dB) and (degree/dB).

It is clear from the above equation that the C/I_3 level of solid state nonlinear amplifiers used in multicarrier communication systems or in communication systems using time varying envelope signals, such as QPSK or QAM signals, can be reduced by minimizing the AM/AM and AM/PM distortions separately. Based on this, two different linearization

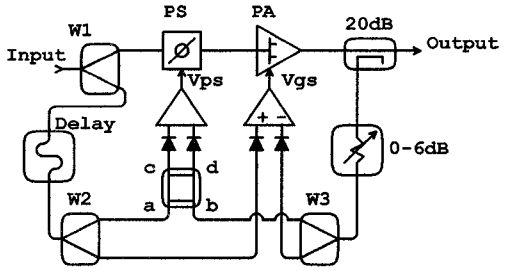

Fig. 2. ADEF amplifier block diagram.

circuits to simultaneously correct for the AM/AM and the AM/PM distortions are incorporated in the ADEF amplifier. Both circuits use envelope feedback. The AM/AM linearization circuit uses dynamic biasing to control the gain [15] while the AM/PM linearization circuit uses a phase shifter for phase control. As shown in the ADEF amplifier block diagram (Fig. 2), the MESFET power amplifier's gate voltage, V_{gs}, and the phase-shifter's voltage, V_{ps}, are controlled separately by two gain and phase envelope feedback signals using zero-bias detectors and operational amplifiers (Op-Amps). The gain variations (AM/AM distortion) are detected directly while the phase variations (AM/PM distortion) are detected through a 90° hybrid junction. These two linearization loops will now be described in detail.

A. AM/AM Distortion Cancellation Loop

AM/AM distortion is reduced by maintaining constant gain over the output power's dynamic range. This can be achieved by dynamically varying the gate voltage, V_{gs}, of the output power MESFET. This is possible since when the gate goes more negative, the MESFET is closer to pinch-off and its gain is reduced. On the other hand, as the gate goes more positive, the MESFET will approach class A, where its gain is maximum. It should be noted that the gain of the Op-Amp driving V_{gs} in Fig. 2 has a direct impact on the AM/AM distortion. Indeed, increasing its gain, G_{op}, will decrease the power difference between its inputs and, consequently, the RF gain variation (AM/AM distortion) will be reduced.

B. AM/PM Distortion Cancellation Loop

AM/PM distortion is reduced by maintaining a constant phase shift between the input and output signals over the ADEF amplifier's dynamic range. Referring to Fig. 2, it can be seen that any phase shift between the amplifier's input and output will create the same phase shift at the input of the branch-line coupler. Let $\boldsymbol{a}$ and $\boldsymbol{b}$ represent the input signals of the branch-line coupler, $\boldsymbol{c}$ and $\boldsymbol{d}$ its output signals, and θ the angle of $(\boldsymbol{b}/\boldsymbol{a})$. Then, for a branch-line coupler we have

$$\boldsymbol{c} = \frac{\sqrt{2}}{2}(\boldsymbol{a} - j\boldsymbol{b}) \quad \text{and} \quad \boldsymbol{d} = \frac{\sqrt{2}}{2}(\boldsymbol{b} - j\boldsymbol{a}). \tag{5}$$

The two outputs of the coupler are then detected by the diodes and their difference is amplified yielding the phase shifter's controlling voltage, V_{ps}, according to the equation

$$V_{ps} = G_{op}(|\boldsymbol{c}|^2 - |\boldsymbol{d}|^2). \tag{6}$$

Combining (5) and (6) gives

$$V_{ps} = G_{op}|\boldsymbol{a}||\boldsymbol{b}| \sin\theta \approx G_{op}|\boldsymbol{a}|\boldsymbol{b}|\theta, \qquad \text{for small } \theta. \tag{7}$$

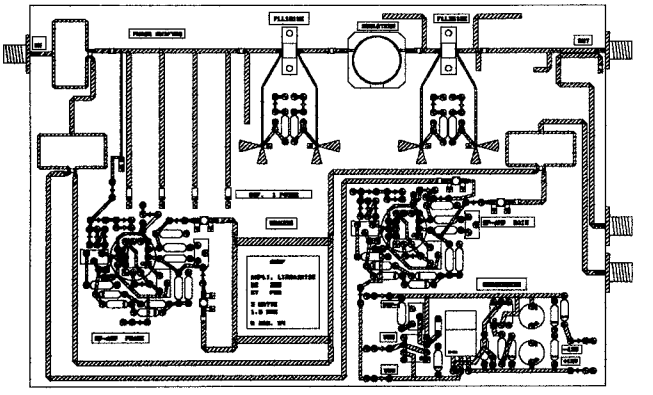

Fig. 3. ADEF amplifier printed circuit board layout.

Based on the above equations, it can be seen that if the gain of the Op-Amp, is large enough, the phase difference, θ, between $\boldsymbol{a}$ and $\boldsymbol{b}$ will be kept very small for any power level. Therefore, the AM/PM distortion will be reduced by this feedback loop. Equation (7) also shows that the amplitudes $|\boldsymbol{a}|$ and $|\boldsymbol{b}|$ must be kept constant which is simultaneously achieved by the AM/AM loop.

Compared to the linearizers mentioned above, the ADEF linearizer presents a simpler approach. Very low power Op-Amps (comparable to the usual Op-Amps used to control the drain current in commercial class A power amplifiers) can be used to drive the phase-shifter and to dynamically bias the gate of the MESFET. In addition, the dynamic bias on the gate of the MESFET, used to control its power gain, results in a 1 dB increase in the $P_{1\text{dB}}$ of the ADEF amplifier by comparison to class AB amplifier (ADEF amplifier when both loops are open). Consequently, the ADEF amplifier will consume practically no additional current in comparison to the same nonlinearized class AB amplifier. Finally the nature of the feedback makes the amplifier adaptive and self-regulatory to drifts in the operating electrical and environmental conditions such as temperature, carrier frequency, input power level, aging and battery level.

III. ADEF Amplifier Detailed Design Description

Block diagram of the ADEF amplifier with its two feedback loops is shown in Fig. 2, where W1, W2 and W3 are single section Wilkinson dividers. The diode detectors and the Op-amp driving V_{gs} in the baseband circuit detects and amplify the envelope-level difference between the input and output of the ADEF amplifier. The branch-line coupler, diode detectors and the Op-amp driving the phase-shifter detect and amplify the relative phase difference between the input and output of the ADEF amplifier.

An L band, two-stage ADEF amplifier was designed and manufactured in MIC technology using a Duroid substrate having a thickness of 20 mil and a relative permittivity equals to $\varepsilon_r = 2.3$. The layout of the complete ADEF amplifier is shown in Fig. 3. All the main blocks described in Fig. 2 can be easily identified in this figure except for the delay line, which was added subsequently, and the variable attenuator, which was implemented externally. The PA is a two stage class AB power amplifier using the Fujitsu FLL101ME as a driver

and the FLL351ME as the output stage. The FLL351ME was characterized using an active load-pull measurement set-up for a class AB bias point [16]. The phase-shifter was designed using four varactor diodes controllable with an analog voltage between -10 and 0 V and producing a 40° tuning range.

Several important considerations must be addressed during the design process in order to meet the desired performance criteria. Such considerations include:

1) Limitations on the PA gain: since the ADEF amplifier gain is maintained constant by the AM/AM loop, selection of the value of the fixed attenuator (0–6 dB) in Fig. 2 must be carefully adjusted to avoid requiring a higher RF gain than what the PA can deliver.
2) Diode detectors' nonlinearity: Matched pairs of diode detectors should be selected at the input of the Op-Amps since any response difference between the two diodes will create extra AM/AM or AM/PM distortions. With identical diodes, the performance of the AM/AM and AM/PM loops will not be affected by the nonlinearities in the V_{out} to P_{in} curves of the diodes.
3) Op-Amps offset voltage setting: when the ADEF amplifier is operated in small signal mode, the inputs to the Op-Amps of the feedback loops are approximately zero. To insure good operating conditions of the loops over the entire dynamic range, small and large signal modes, the offset voltages of the Op-Amps must be adjusted so that the small signal gain and phase shift of the ADEF amplifier are the same as under large signal operating conditions.
4) Frequency bandwidth of the ADEF amplifier: in order to insure that the ADEF amplifier operates over a large RF frequency bandwidth, the electrical length between the two paths that separate the two output ports of W1 and the two input ports of the branch-line coupler a and b, must be equal (see Fig. 2). Therefore, a delay line is inserted between W1 and W2 in order to maintain a zero phase shift between the inputs of the branch-line coupler for any carrier frequency.
5) Input return loss of an amplifier stage under a dynamic bias: S_{11} of any power MESFET depends on the gate bias level. It is then recommended to insert an isolator between the input of the dynamic biased stage and the output of the previous stage in order to avoid a mistuning of the driving stage.

IV. Stability of the Feedback Loops

Since there are two feedback loops in the ADEF amplifier, each loop must be carefully studied in order to insure global stability of both loops. Unfortunately, these loops are not independent. For instance, any variation in V_{gs}, in the AM/AM loop, will produce phase as well as gain variations of the RF signal being amplified by the PA. Similarly, the AM/PM loop can interact with the AM/AM loop if the insertion loss of the phase shifter varies with V_{ps}. Because it is not possible to avoid the phase variations associated with the dynamic bias on the gate of the output stage, it is crucial, for stability purposes, to maintain the insertion loss of the phase-shifter as constant as possible with respect to V_{ps}, eliminating any

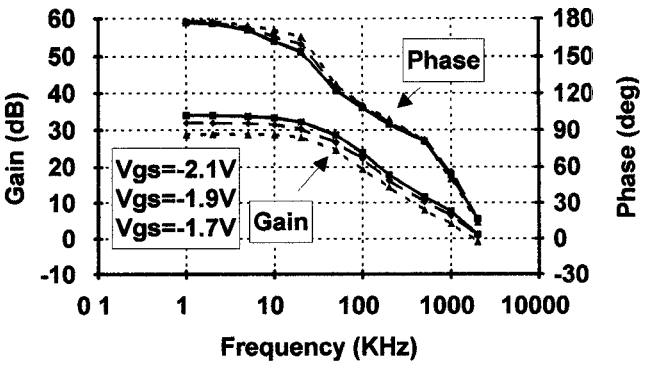

Fig. 4. Bode plots of the AM/AM loop.

double cross-coupling between the loops. The following steps give the procedure used in analyzing the ADEF amplifier's stability:

1) V_{gs} and V_{ps} are disconnected from the Op-Amps.
2) A small sine wave in the KHz region is introduced on top of the dc bias of V_{gs} in the PA.
3) The small-signal open-loop frequency response of the AM/AM loop is measured from V_{gs} to the op-amp output in order to draw a Bode plot. The frequency response is measured form 1 KHz to 2 MHz.
4) Depending on the phase and gain margins on the Bode plot, a frequency compensation filter may be needed at the output of the Op-Amp in order to make the loop stable [17].
5) V_{gs} is reconnected to the AM/AM loop's Op-Amp.
6) Steps 2–5 are repeated for the AM/PM loop between the phase-shifter and its Op-Amp.

The open loop response of the AM/AM loop is shown in Fig. 4. It is interesting to note that the AM/AM loop's gain increases as V_{gs} becomes more negative. This is due to the variation of the operating point created by the small baseband sine wave in step 2. A qualitative explanation of this effect is as follows: a MESFET operating in class B will have its small signal RF gain switched on and off by a small variation in its bias point, while in a class AB, it will have relatively less variation in its small signal RF gain with a small variation in its bias point. Therefore, it can be deduced that the AM/AM loop gain will increase as the MESFET's operating point goes towards class B or C. It is important at this point not to confuse the loop gain with the RF gain, which decreases as V_{gs} becomes more negative. Also from Fig. 4, one can see that the AM/AM loop has a phase margin of 20° degrees when $V_{gs} = -1.7$ V. Therefore this loop alone is comfortably stable and does not need a compensation filter to be inserted between the output of the Op-Amp and the gate of the MESFET.

Fig. 5 shows the open-loop response of the AM/PM loop at $V_{ps} = -2.4$ V. Depending on the phase-shifter used, the response of the second loop can vary greatly. The phase-shifter used in this ADEF amplifier tends to have more effect on the phase when V_{ps} goes more negative. Therefore the 20° phase margin shown in Fig. 5 leads to a minimum value of $V_{ps} = -2.4$ V. If Vps goes below -2.4 V, the phase and gain margins of the AM/PM loop will decrease towards zero and may cause the ADEF amplifier to be unstable around 200 KHz.

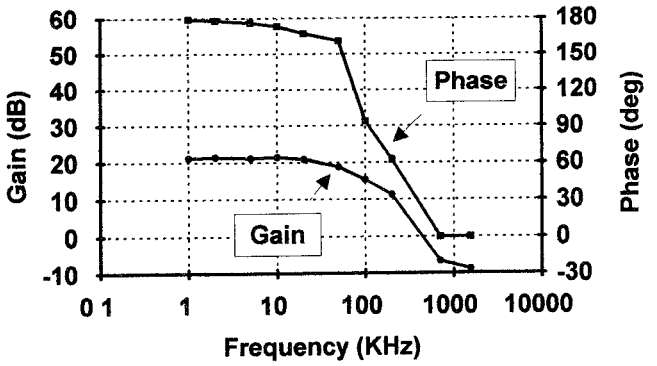

Fig. 5. Bode plot of the AM/PM loop at $V_{ps} = -2.4$ V.

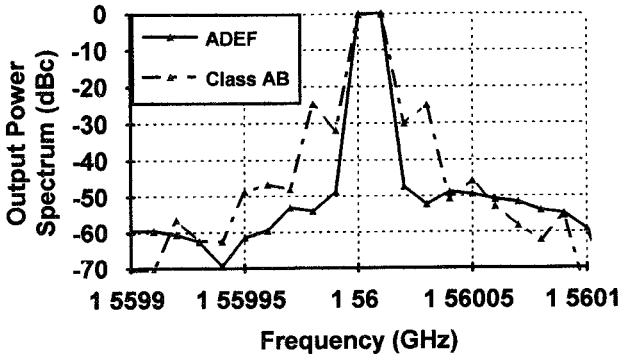

Fig. 6. Power spectrum measured under two-tone test with a 10 KHz frequency spacing for both ADEF and class AB amplifiers.

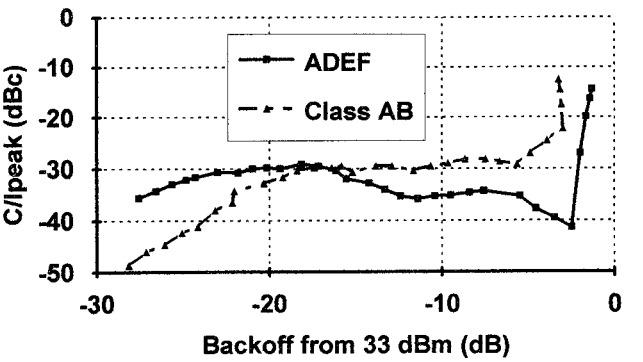

Fig. 7. C/I peak measured under two-tone test with a 10-KHz frequency spacing for both ADEF and class AB amplifiers.

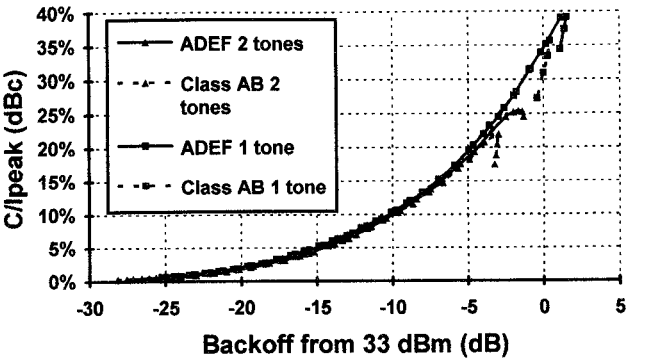

Fig. 8. PAE measured under one tone and two-tone tests for both ADEF and class AB amplifiers.

V. Experimental Evaluation of the ADEF Technique

Evaluation of the prototype performances was carried out by automated measurements while sweeping the input power in 1 dB steps over a 25-dB dynamic range until the PA enters compression. The results showing the performance of the ADEF amplifier are presented in Figs. 6–16. The results obtained are presented as a function of the backoff level of the output power relative to the class AB amplifier $P_{1\text{dB}} = 33$ dBm. Since the independent variable in most of the measurements is the input power, the backoff level used as the abscissa is a dependent variable.

In all figures presented in this section the following conditions apply unless otherwise noted

Carrier Freqency:	1.6 GHz
two-tone spacing:	10 KHz
two-tone offset:	0 dB
Temperature:	35°C.

A. Power Efficiency and Linearity Evaluation

In order to evaluate the ADEF amplifier performance, the main figures of merit such as the IBIP and PAE were measured on both ADEF and class AB amplifiers. The class AB amplifier is the PA shown in Fig. 2 when V_{gs} is fixed at -1.8 V and both loops are open.

Fig. 6 shows the power spectrum for both amplifiers clearly. The ADEF amplifier reduces the 3rd and 5th order IBIP level by approximately 23 dB in comparison with the class AB amplifier. The large frequency bandwidth of the operational amplifiers used in the feedback loops of the ADEF amplifier generates high order IBIPs. For this reason, the worst case situation is retained in these measurements, the level of the IBIPs will be considered as C/I peak which is the ratio of the level of the carriers over the level of the highest intermodulation product falling in a 1 MHz frequency span around the center frequency $((f_1 + f_2)/2)$. Thus, for the class AB amplifier, as shown in Fig. 6, C/I peak $= C/I_5 = -24$ dBc, the 5th order intermodulation product on left of the carrier frequencies. In the case of the ADEF amplifier, as shown in Fig. 6, C/I peak $= C/I_3 = -47$ dBc and it is located to the right of the carriers.

Fig. 7, which gives a plot of the IBIPs for both amplifiers, shows that ADEF amplifier's C/I peak is approximately 7 dB below that of class AB amplifier over a 10-dB output power dynamic range. At the beginning of the saturation region the C/Ipeak reaches 20 dB below that of the class AB amplifier.

Fig. 8 shows the power added efficiency (PAE) results for both amplifiers. The PAE is calculated with the following expression

$$\text{PAE} = \frac{P_{\text{load}} - P_{\text{in}}}{10(I_{ds1} + I_{ds2})} \tag{8}$$

where I_{ds1} and I_{ds2} represents the drain current consumption of the FLL101ME and FLL351ME respectively, both biased at $V_{ds} = 10$ V. It is interesting to notice that, in Figs. 7 and 8, due to the dynamic bias on the gate of power MESFET, the ADEF amplifier $P_{1\text{dB}}$ is 1 dB higher than that of the class AB amplifier. This 1-dB increase in the output power is accompanied by a 4% increase in the over-all PAE of the ADEF amplifier relative to class AB amplifier PAE. However,

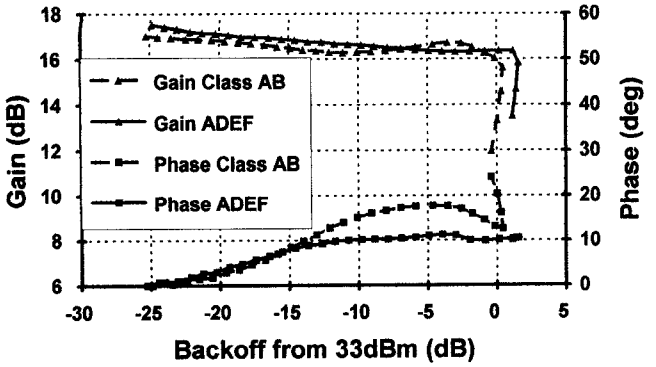

Fig. 9. Gain and phase variation versus P_{out} for both ADEF and class AB amplifiers.

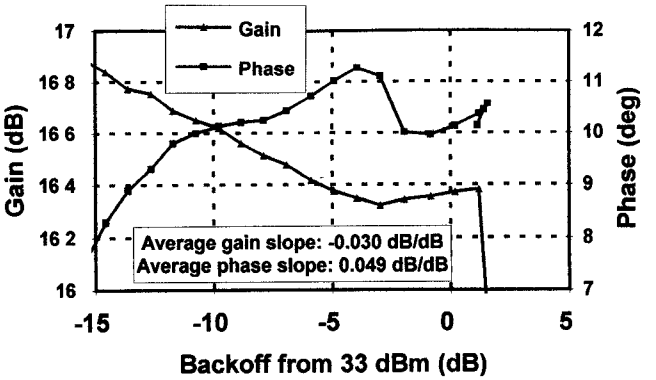

Fig. 10. AM/AM and AM/PM distortion measurements for ADEF amplifier.

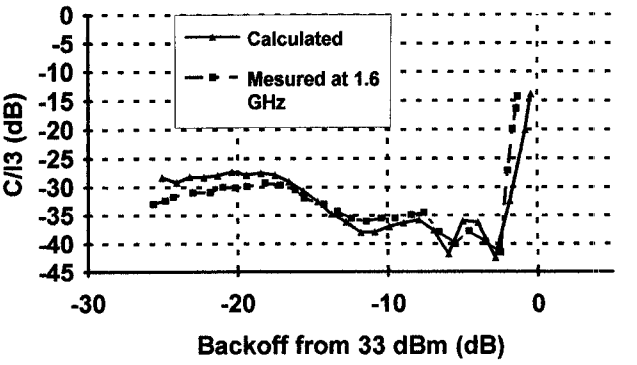

Fig. 11. Measured and calculated C/I_3 using (4) under two-tone test versus P_{out}.

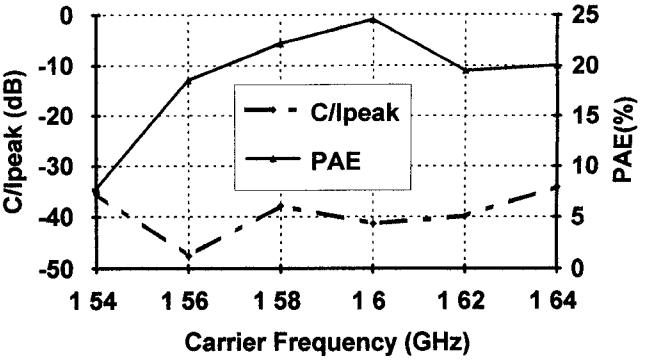

Fig. 12. IBIPs and PAE levels versus RF frequency of ADEF amplifier at −3-dB backoff power level.

to accommodate modulation bandwidths larger than 20 KHz, faster Op-Amps which, in principle, consume more dc power are needed for the operation of the ADEF amplifier. In this case the PAE in expression (8) should include the current consumption of the baseband circuitry.

Fig. 9 shows the gain (AM/AM distortion) and phase (AM/PM distortion) variations of the class AB and ADEF amplifiers with respect to the output power level backoff. It can be seen from this figure that the gain and phase flatness of the ADEF amplifier are improved, particularly, over the last 7 dB before the $P_{1\text{dB}}$. This figure also shows that the feedback loops have a 15-dB dynamic range. In other words the diode detectors and the op-amps start to detect and correct for AM/AM and AM/PM distortions when P_{out} goes higher than −15-dB backoff from $P_{1\text{dB}}$.

B. Experimental Validation of (4)

The results of the experimental validation of the newly developed formula, 4, which relates the AM/AM and AM/PM distortion coefficients of SSPAs to the C/I_3 are presented below. Fig. 10 shows the amount of AM/AM and AM/PM distortions in the ADEF amplifier. This graph is essentially a close-up view of the ADEF amplifier characteristics shown in Fig. 9. In order to estimate the C/I_3 at a given average two-tone output power, the AM/AM and AM/PM distortion coefficients must be calculated at 3 dB above the average two tone power which is the peak output power of an equal two-tone envelope. For example, the C/I_3 at −8 dB backoff can calculated using a linear regression centered at −5 dB over a 20-dB range on both gain and phase response curves. The following parameter values have been obtain

$$G_1 = -0.030 \text{ dB/dB} \quad \text{and} \quad A_1 = 0.049 \text{ deg./dB}. \tag{9}$$

The C/I_3 at −8 dB backoff can be calculated with (4) as follows

$$\frac{C}{I_3} = -10\log\lfloor(0.26 \times 0.03)^2 + (0.047 \times 0.049)^2\rfloor = -42 \text{ dBc}. \tag{10}$$

Repeating this procedure over the entire dynamic range of the ADEF amplifier with 1 dB step, one can obtain the results in Fig. 11. In addition, the coefficients found in (9) show that the G_1 contributes more to C/I_3 than A_1. Consequently, at −8 dB backoff, improvements to the design of the AM/AM loop would have greater impact than improvements to the AM/PM loop.

C. Evaluation of the Adaptive Behavior of the ADEF Technique

The adaptive behavior of the ADEF technique is carried out by monitoring the C/I peak level while monitoring changes in carrier frequency, operating temperature, and two-tone amplitude-offset and spacing. The results obtained are shown in Figs. 12–15.

Fig. 12 shows a 5-dB degradation in ADEF amplifier C/Ipeak performance for a 6% change in the carrier frequency. In principle, the ADEF amplifier RF bandwidth is limited by the RF bandwidths of the components comprising the amplifier. Since the prototype ADEF amplifier described in this paper is a narrow-band design centered at 1.6 GHz, the ADEF technique is only effective over a narrow bandwidth.

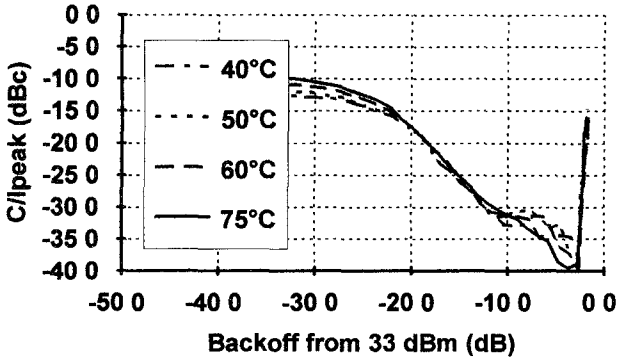

Fig. 13. C/I peak and PAE levels of ADEF amplifier at operating temperatures of 40, 50, 60 and 75°C.

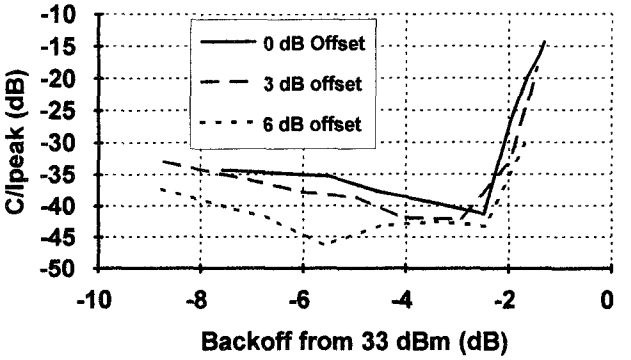

Fig. 14. C/I peak of ADEF amplifier under unequal amplitude two-tone tests for 0, 3, 6 dB amplitude unbalance.

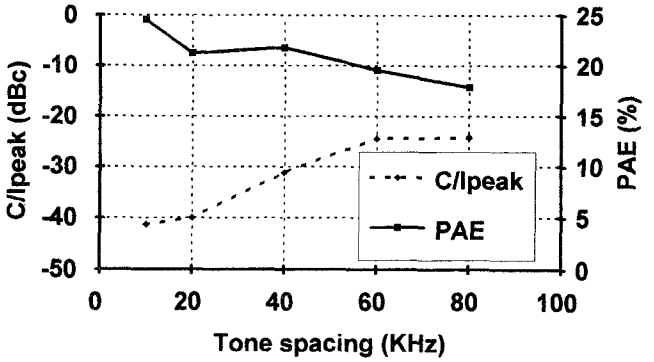

Fig. 15. IBIPs and PAE levels versus frequency spacing between the two-tone of ADEF amplifier at −3-dB backoff power level.

Fig. 13 shows how the ADEF amplifier adapts to the ambient temperature. The amplifier's temperature was raised up to 75°C and only a 5-dB variation in C/I peak was observed. The temperature variation requires special attention during the design of the phase-shifter, since any variation in temperature causes variation in electrical path lengths due to thermal expansion. Since it is relatively difficult to predict the amount of phase shift drift in the rest of the circuit due to temperature variations, the phase-shifter should be designed to cover a larger phase shift range than what the MESFET's AM/PM distortion requires at room temperature.

Fig. 14 shows that a difference in amplitude between the tones in a two-tone test causes a significant change in C/I peak only when this difference becomes larger than 3 dB. Actually, under unequal amplitude two-tone test, the signal envelope becomes more like an offset sine-wave which contains

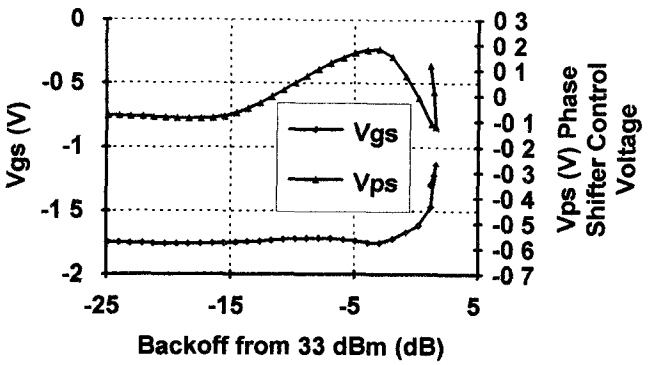

Fig. 16. Variation of MESFET gate and phase shifter voltages, V_{gs} and V_{ps}, as a function of the output power level.

less harmonics than the rectified sine-wave waveform of an equal two tone envelope. Hence, for offsets larger than 3 dB, the ADEF amplifier can operate over a larger modulation bandwidth [19].

Fig. 15 shows the IBIP and the PAE performances of the ADEF amplifier prototype as a function of the two-tone frequency spacing. It can be deduced that in order to keep the ADEF amplifier's IBIPs better than −40 dBc, the two-tone spacing should be kept below 20 KHz. Above this frequency spacing, the IBIP performance suffers from the gain roll-off of the Op-Amps. Faster Op-Amps could be used to increase the modulation bandwidth.

D. Observations

By examining the ADEF amplifier's IBIP in Fig. 7, it can be seen that when the output power is just below saturation C/I peak drops rapidly. This is due to the gain and phase loops becoming more active as power increases.

Fig. 16 shows the variation of the control voltages V_{gs} and V_{ps} versus output power backoff. It is interesting to notice how the V_{ps} curve in Fig. 16 and the phase response curve in Fig. 9 for the class AB amplifier correlate. This demonstrates that the AM/PM loop in the ADEF amplifier presents a good solution for AM/PM distortion cancellation.

In large signal operation, the transmission gain and phase, of the ADEF amplifier are maintained constant by the two feedback loops . Since the power envelope of a two-tone signal varies from 0 to twice of the average power, the detector diodes will not respond to the low power portion of the envelope. Therefore is it important to adjust the voltage offsets of the Op-Amps at low power level where the feedback loops cease to operate to insure that the gain and phase of the ADEF amplifier are constant in both small and large signal operating modes. The effect of the voltage offset in the Op-Amps can also be seen in Fig. 13, where the C/I peak is still very high even when Pout is in the far backoff region. This is due to the fact that the offset of the gain loop Op-Amp was accidentally fixed near −3 V, which drives the PA into a strongly nonlinear class C operating mode when the RF signal is small.

It can be seen in Fig. 8, that three of the PAE curves are curling backwards. This indicates that the output power is decreasing faster than the rate increase in the input power. This is due to the forward bias of the gate to source junction of the MESFET, which occurs at the positive peak of the gate RF

voltage swing and results in a positive dc gate current. This dc current is large enough to override the output current capacity of the Op-Amp, thus pulling down the gate voltage as can be observed for the last two points in Fig. 16. Furthermore, this larger negative dc gate voltage is accompanied by a quick RF gain reduction of the MESFET faster than the increase in the input power. This leads to a decrease in the output power while the input power is increasing as shown in Figs. 7–9 and 16.

VI. Conclusion

A new adaptive double envelop feedback amplifier has been developed and implemented on a two-watt Class AB amplifier. This prototype ADEF amplifier clearly improves the intermodulation performance over a simple class AB amplifier. A two-tone test has shown an average of -40 dBc in C/I peak at 2 dB from 1-dB compression point with a 70 MHz carrier bandwidth and a 20 KHz modulation bandwidth for the ADEF amplifier, compared to an IBIP of -20 dBc for the class AB amplifier under the same conditions. The ADEF amplifier has demonstrated its suitability for indoor/outdoor applications since it is self-adaptive to variations in the operating conditions, such as temperature, carrier frequency and input power level. The dynamic bias on the gate of the MESFET resulted in an increase in $P_{1\text{dB}}$ by 1 dB which improved the PAE by 5%, from 35–40%. While in this experiment the modulation bandwidth was limited to 20 KHz, higher modulation bandwidths can be obtained by using higher speed Op-Amps. The ADEF amplifier's IBIP and PAE performance as well as its stability and simplicity make it more attractive for mobile communications transceivers compared to other linearization methods such as Cartesian feedback, Feedforward, LSA-BC, adaptive DSP predistortion or LINC.

A new accurate formula relating the level of the third-order intermodulation products with the AM/AM and AM/PM distortion coefficients has also been proposed. This new formula has been validated with simulated and experimental results.

Acknowledgment

The authors would like to acknowledge F. Beauregard and N. Constantin and for their helpful discussions and experimental assistance.

References

[1] G. Daniels, "The European market for digital cellular communications," *Microwave J.*, pp. 66–80, Jan. 1993.
[2] I. Shimizu, S. Saito, K. Dhiba, Y. Tarusawa, and Y. Yamao, "New digital mobile radio technologies," *NTT Rev.*, vol. 4, no. 1, pp. 64–69, Jan. 1992.
[3] QPSK in USA, Standards IS-94 and IS-54.
[4] S. Ariyavisitakul and T.-P. Liu, "Characterizing the effects of nonlinear amplifiers on linear modulation for digital portable radio communications," *IEEE Trans. Vehicular Technol.*, vol. 39, no. 4, pp. 383–389, Nov. 1990.
[5] T. Nojima, S Nishiki, and K. Chiba, "High efficiency transmitting power amplifiers for portable radio units," *IEICI Trans.*, vol. E 74, no. 6, pp. 1563–1570, June 1991.
[6] F. J. Casadevall, "The LINC transmitter," *RF Design*, pp. 41–48, Feb. 1990.
[7] A. Bateman, R. J. Wilkinson, J. D. Marvill, "The application of digital processing to transmitter linearization," in *EUROCON 88, 8th Euro. Conf. Electrotechnics*, pp. 64–67.
[8] A. S. Wright and W. G. Durtler, "Experimental performance of an adaptive digital linearized power amplifier," *IEEE Trans. Vehicular Technol.*, vol. 41, no. 4, pp. 395–400, Nov. 1992.
[9] S. Kumar and G. Wells, "Memory controlled feedforward lineariser suitable for MMIC implementation," *IEEE Proceedings*, pt.H, vol. 138, no. 1, pp. 9–12, Feb. 1991.
[10] W. Bösch and G. Gatti, "Measurements and simulation of memory effects in predistortion linearizers," *IEEE Trans. Microwave Theory Tech.*, vol. 37, no. 12, Dec. 1989.
[11] A. P. Lisitskiy and V. V. Nikiforov, "Modeling of minor distortions in an amplifier with correcting amplitude and phase feedback," *Telecommun. Radio Eng.*, pt. 2, pp. 81–83, Dec. 1987.
[12] A. Bosotti, M. D. Giacomo, A. Gallo, and C. Pagani, "Analog control loops for the Milan K800 cyclotron RF system," *Ist. Naz. Fis. Nucl.*, Milan, Italy, Oct. 25, 1989.
[13] M. J. Koch and R. E. Fisher, "A high efficiency 835 MHz linear power amplifier for digital cellular telephony," in *39th IEEE Vehicular Technol. Conf.*, 1989, pp. 17–18.
[14] J. H. Abeles, "Third-order nonlinearity of GaAs MESFET's," in *1984 IEEE MTT-S Dig.*, pp. 224–226.
[15] T. H. Miers and V. A. Hirsch, "A thorough investigation of dynamic bias on linear GaAs FET power amplifiers performance," in *IEEE MTT-S Dig.*, 1992, pp. 537–540.
[16] F. M. Ghannouchi and G. Bosisio, "An automated millimeter-wave active load-pull measurement system based on six-port techniques," *IEEE Trans. Instrum. Meas.*, vol. 41, no. 6, pp. 957–962, Dec. 1992.
[17] B. C. Kuo, *Automatic Control Systems*, 5th ed, Englewood Cliffs, NJ: Prentice-Hall, 1987.
[18] H. Ikeda, T. Ishizaki, Y. Yoshikawa, T. Uwano, and K. Kanazawa, "Phase distortion mechanism of a GaAs FET power amplifier for digital cellular application," in *1992 IEEE MTT-S Dig.*, pp. 541–544.
[19] R. Antepyan, "Analyzing third-order IMD in power amplifiers," *Microwave & RF*, pp. 121–122, Jan. 1994.

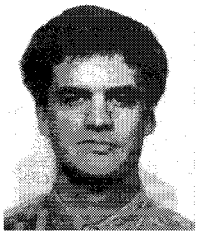

Jean-Serge Cardinal received the B.SC. degree from Ottawa University, Ottawa, Canada, in 1989 and the M.Eng. degree from École Polytechnique of Montréal, Canada, in 1994, both in electrical engineering.

From 1989 to 1992 he worked on image capture circuits for fingerprint scanners at OSCAN Electro-Optics Inc. in Ottawa. Since 1994, He is an Electrical Engineer at S.R. Telecom Inc. in Montréal, Canada, where he is involved in the design of digital radio communication systems.

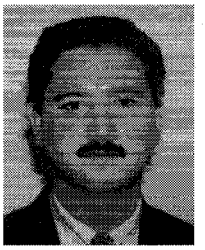

Fadhel M. Ghannouchi (S'84-M'88-SM'93) received the DEUS degree in physics/chemistry in 1980 from the University of Tunis. He received the B.Eng. degree in engineering physics in 1983 and the M.Eng. and Ph.D. degrees in electrical engineering in 1984 and 1987, respectively, from Ecole Polytechnique de Montreal, Montreal, Canada.

He is currently an Associate Professor with the Electrical Engineering Department at Ecole Polytechnique de Montreal where he has been teaching Electromagnetics and microwave theory and techniques since 1984. His current research interests are in microwave/millimeter-wave instrumentation and measurements. He conducted several research projects that led to the design and construction of several six-port network analyzers over the 0.5-40 GHz range. He extended the six-port techniques from standard 5 parameter measurements to multiharmonic load- pull and pulse measurements of microwave active devices and to the control and calibration of phased array antennas. His other research interests are in the area of nonlinear characterization and modeling of microwave and millimeter-wave transistors (MESEET's, HEMT's and HBT's) and in the CAD of nonlinear microwave circuits.

Dr. Ghannouchi is a registered professional engineer in the province of Quebec, Canada. He is a member of the editorial boards of IEEE Transactions on Microwave Theory and Techniques and IEEE Transactions on Instrumentation and Measurement. He served on the technical committees of several international conferences and symposiums and provide consulting services to a number of microwave companies.